

Reinforcement Learning from a Mixture of Interpretable Experts

Riad Akrou¹, Davide Tateo¹, and Jan Peters^{1, 2}

¹IAS, TU Darmstadt, Darmstadt, Germany

²Max Planck Institute for Intelligent Systems, Tübingen, Germany
{riad.akrou, davide.tateo, jan.peters}@tu-darmstadt.de

Abstract

Reinforcement learning (RL) has demonstrated its ability to solve high dimensional tasks by leveraging non-linear function approximators. These successes however are mostly achieved by 'black-box' policies in simulated domains. When deploying RL to the real world, several concerns regarding the use of a 'black-box' policy might be raised. In an effort to make the policies learned by RL more transparent, we propose in this paper a policy iteration scheme that retains a complex function approximator for its internal value predictions but constrains the policy to have a concise, hierarchical, and human-readable structure, based on a mixture of interpretable experts. We show that our proposed algorithm can learn compelling policies on continuous action deep RL benchmarks, matching the performance of neural network based policies, but returns policies that are more amenable to human inspection than neural network or linear-in-feature policies.

1 Introduction

Reinforcement Learning (RL) [1, 2] has led to several practical breakthroughs despite the high dimensionality of the state-action space of the problems at hand [3, 4]. To do so, recent RL algorithms learn complex function approximators, typically 'black-box' deep neural networks [3, 5]. However, the opacity of these function approximators might be a cause for concern, as in some cases the learned policy might need to be scrutinized to ensure that it is safe, ethical and fair. In contrast, a human-readable policy might facilitate these steps by making the learned behavior completely transparent. In addition, a human-readable policy can help the human in understanding and learning the task. For instance, in the Rubik's cube puzzle, while it might be challenging to some, one can consult publicly available policies when stuck, find the state in which they are and take the corresponding action to progress. We propose in this paper an RL algorithm that returns a mixture of expert policy that resembles the Rubik's cube one.

From a learning theory point of view, a human-readable policy will be simpler and hence policies returned by our algorithm might generalize better. RL algorithms use function approximators for estimating the value function [3, 6] or both the value function and the policy [7, 5, 8]. For the sake of interpretability, we propose to replace the policy, with a more interpretable structure. We choose to use an interpretable structure for the policy instead of the value function because the policy usually has a simpler functional shape [9, 10], and can thus be more easily approximated. Our proposed algorithm yields a clustering of the state space, where a single action is associated with each cluster. Such clustering of the state space could be seen as a form of state abstraction [11–14]. Previous work in high-dimensional state abstraction however, only considered non-interpretable state-to-cluster mappings, in the form of polynomial functions [13] or neural networks [14].

As a computer program, the policy returned by our algorithm can be seen as a sequence of `IF` blocks having the structure `IF close(state, center[k]) DO action[k]`; where `state` is the current state, `center[k]` is a cluster center and `action[k]` its associated action. To ensure that such a policy is interpretable, we impose a series of limitations that make the underlying optimization problem challenging. First, we limit beforehand the number of clusters to a fixed (small) number K . Second, and most importantly, we do not allow the cluster centers to be optimized. Instead, we only allow cluster centers to be picked from the stream of states encountered during learning. Doing so ensures that the cluster centers are within the potentially

lower-dimensional manifold that is the state space and hence, are interpretable. The final component that is critical for interpretability is the function `close` that discriminates if a state belongs to the specified cluster, i.e., the state is sufficiently close to the cluster prototype. In this paper, we assume that this function is known. We leave the problem of learning an appropriate distance to future work.

2 Related work

There are two main ways of achieving interpretability in supervised learning: i) learning a black-box model and making it interpretable post-hoc by sensitivity analysis or by (locally) mimicking the black-box with an interpretable model [15–17] or ii) by learning an interpretable model from the get-go such as linear models, decision trees or attention-based networks [18–20]. In RL, a similar categorization exists, where prior work either considered explaining learned policies [21, 22], learning an interpretable policy by imitation learning of a neural network policy [23, 24] or learning an interpretable policy from scratch using for example linear policies [25].

However, we believe that the choice of learning an interpretable structure from scratch is more appropriate than making it interpretable post-hoc, due to the intrinsic sequential nature of RL. First, there is an inherent difficulty in imitating a complex policy with a simpler model, and the unavoidable differences will compound quadratically w.r.t. the problem’s horizon, due to a drift in state distributions [26]. This drift in state distributions renders a local interpretation—i.e. an interpretation w.r.t. a given state—less informative than in supervised learning where the input data distribution is unaffected by the change to a simpler model. Finally, given the fixed complexity of an interpretable policy, typically lower than that of a neural network, the policy might need to adopt a vastly different strategy—e.g. crawling vs running—to the problem; by learning an interpretable policy with RL, we ensure that an optimal policy w.r.t. the particular interpretable policy class is within reach of the learning algorithm.

Decision trees are interpretable structures, and there has been prior work on learning decision tree policies with RL such as with the Fitted Q Iteration (FQI) algorithm [27]. However, learning small enough trees to be interpretable was only demonstrated using imitation learning [24, 28], where a significant reduction in tree size was obtained compared to FQI [24]. As for linear policies, it is important to note that by linear policies we mean linear-in-state as opposed to linear-in-feature, which might perform better [29], but introduces complex transformations of the state space, hindering interpretability. An example of an interpretable linear policy is in the work of [25], where a medical treatment policy was learned. The policy was easy to observe globally as the state was two dimensional. But linear-in-state policies are not always an ideal choice for human-readable policies. First, their interpretability in higher dimensional spaces can be questionable especially when they are not sparse. Secondly, a linear policy class might severely limit the quality of the policy. In this paper, we explore an alternative policy structure akin to nearest neighbors and (Gaussian) kernel-based models. The policy complexity can be increased to match the complexity of the problem but unlike decision trees, part of the policy is differentiable and easier to train.

Kernel-based RL methods have already been explored in the past, such as in the work of [30] that is especially related to ours. Specifically, [30] developed a kernel-based extension of least squared policy iteration [31] and added a compression step to limit the complexity of the policy. Keeping the complexity low is key to providing a human-readable policy. However, in their experiments, more than 3000 centers were used for a double pendulum task with a 4-dimensional state space. In contrast, we are able to learn a walking gait on the `AntBulletEnv-v0` environment, that has a 28-dimensional state space, with as little as 10 centers. To the best of our knowledge, no other kernel-based RL approach has achieved this level of policy simplicity on a task of this complexity.

3 Preliminaries

A Markov Decision Process (MDP) is defined as a 6-tuple $\mathcal{M} = \langle \mathcal{S}, \mathcal{A}, \mathcal{P}, \mathcal{R}, \gamma, \iota \rangle$, where \mathcal{S} is the state space, \mathcal{A} is the action space, assumed to be both continuous spaces, $\mathcal{P} : \mathcal{S} \times \mathcal{A} \times \mathcal{S} \rightarrow \mathbb{R}$ is the transition distribution where $\mathcal{P}(s'|s, a)$ is the probability density of reaching state s' when performing action a in state s , $\mathcal{R} : \mathcal{S} \times \mathcal{A} \rightarrow \mathbb{R}$ is the reward function, $\gamma \in (0, 1]$ is the discount factor, and $\iota : \mathcal{S} \rightarrow \mathbb{R}$ is the initial state distribution. A stochastic policy $\pi : \mathcal{S} \times \mathcal{A} \rightarrow \mathbb{R}$ is a function such that the probability density of taking action

a in state s is $\pi(a|s)$. Let $Q^\pi(s, a) = \mathbb{E}_{s_t, a_t \sim \mathcal{P}, \pi} [\sum_{t=0}^{\infty} \gamma^t R(s_t, a_t) \mid s_0 = s, a_0 = a]$ be the the action-value function of policy π . Let $V_\pi(s) = \mathbb{E}_{a \sim \pi(\cdot|s)} [Q_\pi(s, a)]$ and $A_\pi(s, a) = Q_\pi(s, a) - V_\pi(s)$ be, respectively, the value and the advantage function of π .

A parametric policy is a family of policies π_θ such that the probability distribution depends on a vector of parameters θ . Let $\mathcal{J}(\pi_\theta) = \mathbb{E}_{s_0 \sim \iota} [V_{\pi_\theta}(s_0)]$ be the performance of the parametric policy π_θ and $\pi_{\theta^*} = \arg \max_{\pi_\theta} \mathcal{J}(\pi_\theta)$ be the optimal policy. In this work, we use the Approximate Policy-Iteration (API) framework [32, 33] to find the optimal policy π_{θ^*} . At each iteration we sample trajectories, evaluate the policy and update the policy parameters. The presentation of the paper focuses on the policy update step, since the sampling and policy evaluation steps use instead standard techniques. Specifically, the advantage function of the current policy is evaluated on the generated samples by learning a neural approximated value function, following standard procedures described in e.g. [34].

4 Mixture of interpretable experts policy

We describe more formally in this section the policy structure and the associated learning algorithm. The policy samples an action by comparing the current state to a list of fixed size K of cluster centers $\mathcal{C} = \{s_0, \dots, s_{K-1}\}$. It can then, for instance, select the action associated with the closest cluster. This would yield a discrete optimization problem. However, learning a satisfactory policy in this setting is a challenging problem. We relax our model, by considering instead a smoothed version of the previous problem with fuzzy memberships [35] to each cluster, akin to a mixture of expert approach [36].

Formally, the policy at state s is a Gaussian distribution $\pi(a|s) = \mathcal{N}(a|\mu(s), \Sigma)$ with mean given by

$$\mu(s) = M \frac{w(s)}{\|w(s) + 1\|_1}, \quad w(s) = c \odot \varphi(s), \quad (1)$$

where M is a $K \times \dim(\mathcal{A})$ matrix containing the associated action to each cluster or expert, $w(s)$ is the vector of unnormalized cluster memberships, $\|\cdot\|_1$ the ℓ_1 norm, c is the cluster weights parameter vector, $\varphi(s)$ is the vector of distances to each cluster center, and the operator \odot represents the Hadamard, i.e. element-wise, product. For each cluster center s_i , the distance is computed as

$$\varphi_i(s) = \exp(-\tau \|s - s_i\|_2^2), \quad (2)$$

where $\|\cdot\|_2$ is the Euclidian norm and τ is a fixed temperature parameter.

A final component of the policy is the default action. When a state is far from all cluster centers, the policy becomes too sensitive to small changes in the state variables. This sensitivity introduces both numerical problems and hinders interpretability. We thus introduce a default action, with unnormalized membership fixed to one, independently of the input state. For simplicity we will assume that the value of the default action is fixed to the null vector. This leaves M unchanged and simply requires the additional 1 shown in the denominator of Eq. (1). The benefits in terms of interpretability of the default action is to be able to know when the policy is presented with an unfamiliar state, in which case the sum of the normalized membership $\sum_i w_i(s) \|w(s) + 1\|_1^{-1}$ will be low. In contrast, without the default action, the sum $\sum_i w_i(s) \|w(s)\|_1^{-1}$ will always be equal to one.

The policy structure is simple but the main challenge that it presents is to find an appropriate set of cluster centers \mathcal{C} during learning. As we strive for human-readable policies, the difficulty of this discrete optimization problem is exacerbated by the necessity to keep $|\mathcal{C}|$ small.

5 Learning the mixture of interpretable experts policy

Our algorithm is presented in Alg. 1, and is based on the API scheme [32, 33]. Line 3 to 8 are the initialization and policy evaluation steps while Line 9 to 20 are about the policy update.

5.1 Initialization and policy evaluation

The policy is initialized with the first state encountered as an initial cluster. All cluster weights vector are initialized to zero, excluding the weight for the first cluster, which is initialized to 1. The cluster action means

Algorithm 1 Learning interpretable policies

```
1: Input: environment  $\mathcal{M}$ , Initial value function  $V$ 
2: for it  $\leftarrow 0$  to  $N$  do
3:    $\mathcal{T} \leftarrow \text{generateTrajectories}(\mathcal{M}, q)$ 
4:    $A \leftarrow \text{computeGAE}(q, V)$ 
5:    $V \leftarrow \text{updateValueFunction}(V, A)$ 
6:   if it = 0 then
7:      $q \leftarrow \text{addClusters}(q, \mathcal{T}, A)$ 
8:   end if
9:   if it mod 2 then
10:     $\pi \leftarrow \text{updateFullPolicy}(q, \mathcal{T}, A)$ 
11:   else
12:     $\pi \leftarrow \text{swapClusters}(q, \mathcal{T}, A)$ 
13:     $\pi \leftarrow \text{compressPolicy}(\pi, q, \mathcal{T}, A)$ 
14:    if  $\pi \neq q$  then
15:       $\pi \leftarrow \text{updateMeanAndCovariance}(\pi, q, \mathcal{T}, A)$ 
16:    else
17:       $\pi \leftarrow \text{updateFullPolicy}(q, \mathcal{T}, A)$ 
18:    end if
19:  end if
20:   $q \leftarrow \pi$ 
21: end for
22: return  $\pi$ 
```

are initialized to zero. After generation of the first iteration’s trajectories and after the advantage function is estimated, the other cluster centers are initialized by selecting the $K - 1$ clusters and cluster actions from the state-action couples with the highest advantage value in the collected dataset. This operation does not change the policy distribution as the cluster weights for the uninitialized clusters are set to zero.

Regarding policy evaluation, the sampling and the Generalized Advantage Estimation (GAE) are performed in Alg. 1 by the *generateTrajectories* and the *computeGAE* procedures respectively. The initial cluster center selection is performed by the *addClusters* procedure. As done in other standard API algorithms [8, 37], we generate trajectories rollouts from the environment before estimating the advantage function using the GAE algorithm [34]. What remains, given the advantage value estimated for every state-action pair in the dataset is to update the policy.

5.2 Policy update

The policy update can be divided into two optimization categories, a differentiable optimization problem where we optimize the policy parameters that are the cluster action matrix M , the cluster weights c , and the policy variance Σ , and a discrete optimization problem where we update the cluster center lists \mathcal{C} . In the following, we describe these two optimization problems in details.

5.2.1 Discrete optimization

In the discrete optimization phase, we seek to update the cluster list \mathcal{C} , which is the basis for the computation of the cluster distances φ and the policy mean $\mu(s)$. To retain the interpretable nature of our policy, we enforce the cluster list to contain only states generated by the environment. To illustrate the importance of this constraint, consider an autonomous driving car policy that has an image as input. Allowing the cluster centers to be optimized by gradient descent will result in cluster centers exiting the manifold of human understandable images. In contrast, enforcing the cluster list to only contain images encountered by the autonomous car will facilitate the analysis of the policy by a human and show which prototypical real-world situations make the autonomous car decide on a particular action.

However, as the set of possible states is a discrete set, optimizing the cluster list becomes more challenging and the policy cannot be trained ‘end-to-end’ by gradient descent. As such we separate the optimization of \mathcal{C} from the optimization of M , c and Σ . To optimize \mathcal{C} we need to answer two questions, which objective to

optimize and with which optimization algorithm. We have evaluated several such objectives, including the maximization of the advantage value, a typical choice in policy update. However, we have obtained better results with objectives that favor the spread of the cluster centers and their coverage of the state space, while performing the maximization of the advantage during the differentiable optimization phase.

To maximize coverage we have first considered to maximize $\mathbb{E}_{s \sim q} \sum_i w_i(s) \|w(s) + 1\|_1^{-1}$, i.e. to have cluster centers spread in such a way that the default action is executed as infrequently as possible. However, this has resulted in having several clusters clamped close to each other, possibly around states frequently visited by q , to reduce the influence of the default action. Instead, a better solution would be to keep one cluster in the same area and increase its cluster weight in the differentiable optimization phase.

The optimization criterion that ended-up providing the best results fulfills the following two criteria: it does not depend on parameters optimizer in the differentiable optimization phase and it penalizes clusters being close to each other. This criterion is given by

$$\mathbb{E}_{s \sim q} \left[\varphi_{t_1}(s) - \frac{1}{N} \sum_{i=1}^N \varphi_{t_i}(s) \right], \quad (3)$$

where t is an ordering of $\varphi(s)$ in descending order such that $\varphi_{t_1}(s) = \max_i \varphi_i(s)$, $\varphi_{t_2}(s)$ has the second highest value and so on. For the hyper-parameter N we have tried three values $N = 2$, $N = 3$ and $N = K$ and the best performance was achieved with $N = 3$.

Regarding the discrete optimization of the objective, the high number of possible candidates, that is the set of all states encountered so far or even just the states generated by the current policy, prevents an exhaustive search of all possible combinations, that can be exponential in the number of candidate states. Another aspect complicating the optimization process is the Kullback-Leibler Divergence (KL) constraint later introduced in Sec. 5.2.2 that prevents drastic changes to the policy from one iteration to another. To tackle this challenging optimization problem we resort to approximate techniques by using random search.

The `swapClusters` routine (in Line 12 of Alg. 1) will perform a random search in the cross set of states sampled by q and the states in the current cluster list \mathcal{C} . The routine is composed of a two-step randomization scheme. In the first step, a prioritized sampling using a heuristic function h_1 is used to sample a set of k cluster centers from \mathcal{C} to be swapped with k state candidates sampled from the generated trajectories \mathcal{T} , using a similar sampling algorithm but with a heuristic h_2 .

Both steps are based on the polynomial randomization scheme presented in [38]. The heuristic h_1 to select the cluster center to be replaced and the heuristic h_2 to sample possible candidates are given by

$$h_1(s_i) = \mathbb{E}_{s \sim q} \left[w_i(s) \|w(s)\|_1^{-1} \right], \quad h_2(s) = \|\varphi(s)\|_1.$$

The heuristic h_1 favors clusters with low activation (candidates are ranked in descending order, lower heuristic value is better). We take into account the cluster weights since h_1 is also about selecting clusters that are not likely to violate the KL-divergence constraint if swapped, and the KL-divergence greatly depends on the cluster weight. On the other side, h_2 favors states that are far from the current cluster centers.

Using this randomization scheme we generate a set of n candidates. For every candidate, we check that the obtained policy does not violate the KL-divergence constraint and pick the one with the highest objective in Eq. (3). To perform the maximum number of swaps, we repeat the sampling multiple times, starting from K total swaps i.e., swapping all clusters, and halving the number of swaps if the randomization cannot improve w.r.t. the objective in Eq. (3).

Despite the objective in Eq. (3) penalizing overlap of clusters, it can still happen that the clusters are too close to each other which hinders the expressiveness of the policy. To overcome this problem we add a routine `compressPolicy` that is executed after the swapping routine. The compression takes a simple form, where we try to delete every cluster by setting its cluster weight to 0, and keeping the resulting policy if the KL-divergence constraint is not violated.

5.2.2 Differentiable optimization

The policy parameters—cluster weights, cluster actions, and covariance—are updated by solving the following constrained optimization problem

$$\arg \max_{\pi} \quad L(\pi), \quad (4)$$

$$\text{subject to} \quad \mathbb{E}_{s \sim q} [\text{KL}(\pi(\cdot|s) \parallel q(\cdot|s))] \leq \epsilon, \quad (5)$$

$$\mathbb{E}_{s \sim q} [\mathcal{H}(\pi(\cdot|s))] \geq \beta, \quad (6)$$

where q is the data generating policy. The objective of the problem $L(\pi) = \mathbb{E}_{s \sim q} \left[\frac{\pi(a|s)}{q(a|s)} A_q(s, a) \right]$ is to maximize the expected advantage function. The constraints are a KL constraint between successive policies—akin to a step-size—and an entropy constraint—to sustain exploration. The entropy constraint is especially important in our case since the policy expressiveness is initially quite limited. Indeed, as described in Sec. 5.1, the cluster center list \mathcal{C} initially only contains the first encountered state as an active cluster—i.e. with non-zero cluster weights. Policy improvements on the objective will initially be quite modest compared to a more intricate model and the entropy constraint helps in sustaining exploration while a more representative cluster center list \mathcal{C} is learned.

To tackle the constrained optimization problem we extend the Projections for Approximate Policy Iteration (PAPI) techniques proposed in [39] to our specific policy structure. Specifically, Alg. 2 in PAPI proposes a differentiable projection that projects the parameters of any linear-Gaussian—i.e. a Gaussian distribution for which the mean is a linear function of some state features ϕ —of shape $\pi(a|s) = \mathcal{N}(a|M\phi(s), \Sigma)$, to a linear-Gaussian that complies with constraints (5) and (6). Since this projection is differentiable, the composition of the objective L and the projection can then be optimized using gradient ascent in an unconstrained way.

The projection in PAPI works by linearly interpolating the parameters of the input policy, M and Σ , with the parameters of the data generating policy q . To be able to optimize our policy with similar techniques, we need to provide a projection of the policy parameters that takes into account the cluster weights. Since the cluster weights in our policy only affect the mean of the Gaussian, the entropy constraint in Eq. 6 will not be affected by a change in cluster weight. As for the KL, since $\pi(\cdot|s)$ and $q(\cdot|s)$ are Gaussians, their KL can be expressed in closed form and is given by

$$\text{KL}(\pi(\cdot|a) \parallel q(\cdot|a)) = \frac{1}{2}m(\mu(s)) + \frac{1}{2}r(\Sigma) + \frac{1}{2}e(\Sigma),$$

where $m(\mu(s)) = \|\mu(s) - \mu_q(s)\|_{\Sigma_q^{-1}}^2 = (\mu(s) - \mu_q(s))^T \Sigma_q^{-1} (\mu(s) - \mu_q(s))$ is the change in mean, $r(\Sigma) = \text{tr}(\Sigma_q^{-1}\Sigma) - d$ is the rotation of the covariance and $e(\Sigma) = \log \frac{|\Sigma_q|}{|\Sigma|}$ is the change in entropy. In the KL, only m depends on s . For clarity of notations, we drop the dependence on s for now, and further expand m into

$$m(\mu) = \left\| M \frac{w}{\|w\|_1} - M_q \frac{w_q}{\|w_q\|_1} \right\|_{\Sigma_q^{-1}}^2,$$

where we have also dropped for clarity, and without loss of generality, the default action contribution, that can be thought of as integrated to w .

Now, given the cluster weights c and cluster actions M of an arbitrary policy that violates the constraint in Inq. (5), we want to find a 'projected' policy π' that has new cluster weights and cluster actions of the form $c_\eta = \eta c + (1 - \eta)c_q$ and $M_\nu = \nu M + (1 - \nu)M_q$ such that $\mathbb{E}_{s \sim q} [\text{KL}(\pi'(\cdot|s) \parallel q(\cdot|s))] \leq \epsilon$. To do so, we will write the constraint in Inq. (5) in terms of the interpolation parameters ν and η , and solve for these parameter $\mathbb{E}_{s \sim q} [\text{KL}(\pi'(\cdot|s) \parallel q(\cdot|s))] = \epsilon$. We know that such a solution exists since the KL-divergence is zero for $\eta = \nu = 0$, is $> \epsilon$ for $\eta = \nu = 1$ and is continuous in η and ν . Unfortunately, efficiently solving this equation is not possible since no closed form exists. However, it is important that the projection is efficient to compute since it is called several times during the policy update. What we propose instead is to derive an upper bound $u(\nu, \eta)$ of $\mathbb{E}_{s \sim q} [\text{KL}(\pi'(\cdot|s) \parallel q(\cdot|s))]$ that has a simpler form in η and ν and solve for these parameters the equation $u(\nu, \eta) = \epsilon$ in closed form and in an efficient manner.

Since only m in the KL-divergence depends on the policy mean, we let $m(\nu, \eta)$ be the change in mean for π' , i.e.

$$m(\nu, \eta) = \left\| M_\nu \frac{w_\eta}{\|w_\eta\|_1} - M_q \frac{w_q}{\|w_q\|_1} \right\|_{\Sigma_q^{-1}}^2$$

where again we have dropped for now the dependency on s . From now on, we will consider the projection in terms of the unnormalized cluster memberships w . Indeed, a suitable η for w is also a valid interpolation for c , due to their linear dependency.

By expanding the square, $m(\nu, \eta)$ can be decomposed into

$$m(\nu, \eta) = \nu^2 \left\| (M - M_q) \frac{w_\eta}{\|w_\eta\|_1} \right\|_{\Sigma_q^{-1}}^2 + 2\nu \left((M - M_q) \frac{w_\eta}{\|w_\eta\|_1} \right)^T \Sigma_q^{-1} \left(M_q \left(\frac{w_\eta}{\|w_\eta\|_1} - \frac{w_q}{\|w_q\|_1} \right) \right) + \left\| M_q \left(\frac{w_\eta}{\|w_\eta\|_1} - \frac{w_q}{\|w_q\|_1} \right) \right\|_{\Sigma_q^{-1}}^2,$$

where the first term is due to the change of cluster action, the last term to the change in cluster weights and the second term is a cross term. The last term is equivalent to $m(0, \eta)$ and can be further decomposed into

$$m(0, \eta) = \frac{\eta^2 \|w\|_1^2}{\|\eta w + (1 - \eta)w_q\|_1^2} m(0, 1).$$

$m(0, \eta) = \epsilon$ still does not admit an easy solution but we derive the following two upper bounds for it

$$m(0, \eta) \leq \eta^2 \max \left(\frac{\|w\|_1^2}{\|w_q\|_1^2}, 1 \right) m(0, 1), \quad (7)$$

$$m(0, \eta) \leq \eta \frac{\|w\|_1^2}{2\|w_q\|_1 \|w\|_1 - \|w_q\|_1^2} m(0, 1). \quad (8)$$

Inq. (7) always holds while Inq. (8) only holds if the denominator is positive. Both bounds have now an easy solution η , as they are quadratic or linear functions of η . We use both the bound in Inq. (7), which is tighter when $\|w\|_1 \approx \|w_q\|_1$, and the bound in Inq. (8), which is tighter when $\|w\|_1 \gg \|w_q\|_1$ by simply taking the one that offers the largest η , i.e. for which the KL-divergence of π' will be the closest to ϵ .

Being able to find an η s.t. $m(0, \eta) \leq \epsilon$ gives us now a path to find a projected policy that complies with the KL-divergence constraint. Given arbitrary cluster weights c and cluster actions M encountered during gradient ascent in the policy update, we define the projection as follow: first fix M to M_q and find an η solution of $m(0, \eta) \leq \epsilon$. Given this η , fix the cluster weight to c_η and compute the resulting state features $\phi(s) = \frac{w_\eta(s)}{\|w_\eta(s) + \mathbf{1}\|_1}$ and then use Alg. 2 of PAPI [39], to find ν . This second step would also project the input Σ such that the overall KL-divergence—including the terms $r(\Sigma)$ and $e(\Sigma)$ that we have omitted so far—and the entropy constraint are satisfied. Since these parts do not depend on the cluster weights, we can reuse the projections of PAPI as is.

The upper bounds of $m(0, \eta)$ are derived for a single s but the KL-divergence constraint is in expectation of states generated by q . Letting m_s be the mean shift of the KL-divergence component at state s , bounding the expected KL-divergence w.r.t. states of q will require to bound $\mathbb{E}_{s \sim q} [m_s(0, \eta)]$. However, the expectation still yields upper bounds easy to solve for, since η^2 and η can simply be taken out of the expectation and the remaining quantities can be evaluated from trajectories.

In Alg. 1, there are two types of policy updates: `updateMeanAndCovariance` that is called if a cluster center is swapped or deleted and `updateFullPolicy` that is called otherwise. When the cluster list \mathcal{C} is modified, we cannot apply the projection for the cluster weights. Indeed, even if Inq. (7) and Inq. (8) still hold and we can find an η to bring m under ϵ , we cannot translate the interpolation in w to an interpolation in c anymore since the cluster distances φ have changed. As such, we resort in this case to only updating M and Σ of the policy in `updateMeanAndCovariance`. To ensure that the cluster weights are learned, we only update the cluster list every second iteration and perform a full update of all differential parameters of the policy otherwise. Note that there is still a chance, especially in later iterations, that the discrete optimization cannot improve over the current cluster list in which case, as shown in Line 17 of the algorithm, a complete update of the policy parameters is performed.

Because of the change to the cluster list \mathcal{C} , simpler and more common approaches such as TRPO [8], that perform policy update under a KL-divergence constraint, cannot be used in our case. Indeed, the theoretical framework of TRPO requires that the KL-divergence constraint is approximated around the data generating

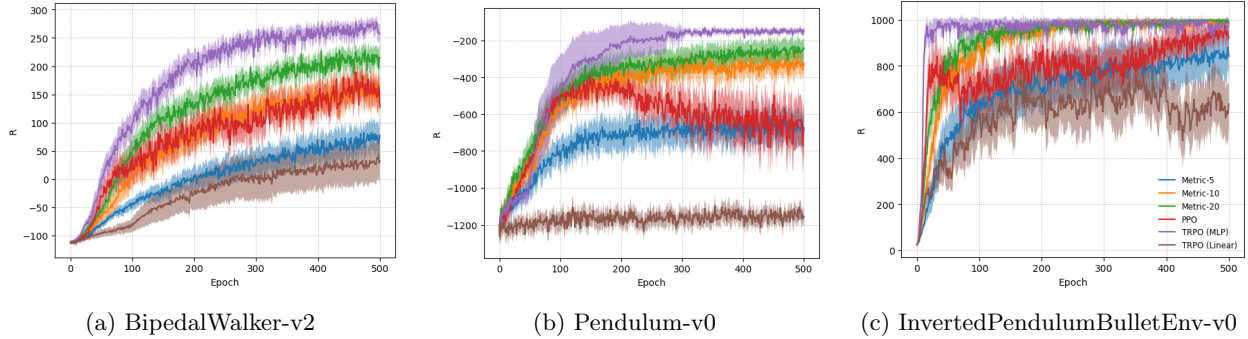


Figure 1: Performance of the interpretable algorithm on three additional Openai-Gym environments. Our algorithm is run with 5, 10 and 20 clusters, and compared to TRPO and PPO with a neural policy and TRPO with a linear policy. Plots show the average reward and 95% confidence interval, out of 25 independent runs.

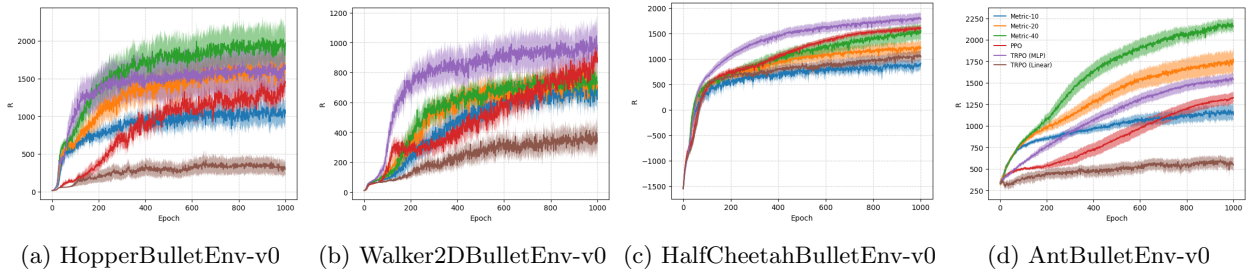


Figure 2: Performance of the our algorithm on four `pybullet` locomotion tasks with 10, 20 and 40 clusters. Our algorithm is compared to PPO, and TRPO with neural network and linear policy. All plots average over 25 runs, showing mean and 95% confidence interval.

policy q whereas we want to update the parameters of a policy with a different cluster list. This policy is not q anymore even when all differentiable parameters are the same. Even though the complexity of the proposed policy update might not be desirable, its payoff is an algorithm that is competitive with TRPO on many RL tasks even when a simpler policy is being used.

6 Experimental Evaluation

The objectives of this section are to assess on one side the performance of our algorithm as an RL learner in comparison to existing methods, and on the other side the extent with which the returned policies can be understood and are human readable. We compare our algorithm to three RL baselines on 7 standard continuous action tasks, and analyze the interpretability of the policy on the four higher dimensional locomotion tasks of `pybullet` [40]. We compare our algorithm to TRPO [8] as it implements a similar, KL-constrained, policy update and to PPO [37]. Both PPO and TRPO are learning a two hidden layer policy with 64 neurons in each layer, as this is the default for these tasks. In addition to the neural network policy, we learn using TRPO a linear policy. This setting is very similar to the work of [29] that demonstrated that linear-in-features—Random Fourier features—policies and linear-in-state policies can perform well on `Mujoco` [41] tasks. These policies were trained using natural gradient descent [42, 43] which is close to TRPO up to a line-search operation. However, the `Mujoco` tasks are generally easier than their `pybullet` counter-parts as the models are physically heavier in the `pybullet` task. The implementation of both TRPO and PPO uses OpenAI’s `baselines` [44].

We will reference to Alg. 1 in the plots as `Metric` and experiment with three different values of the number of clusters K . In the easier tasks, we use $K \in \{5, 10 \text{ and } 20\}$ and on the higher dimensional `pybullet` locomotion tasks we use $K \in \{10, 20, 40\}$. In each experiment, the results are averaged over 25 runs. The

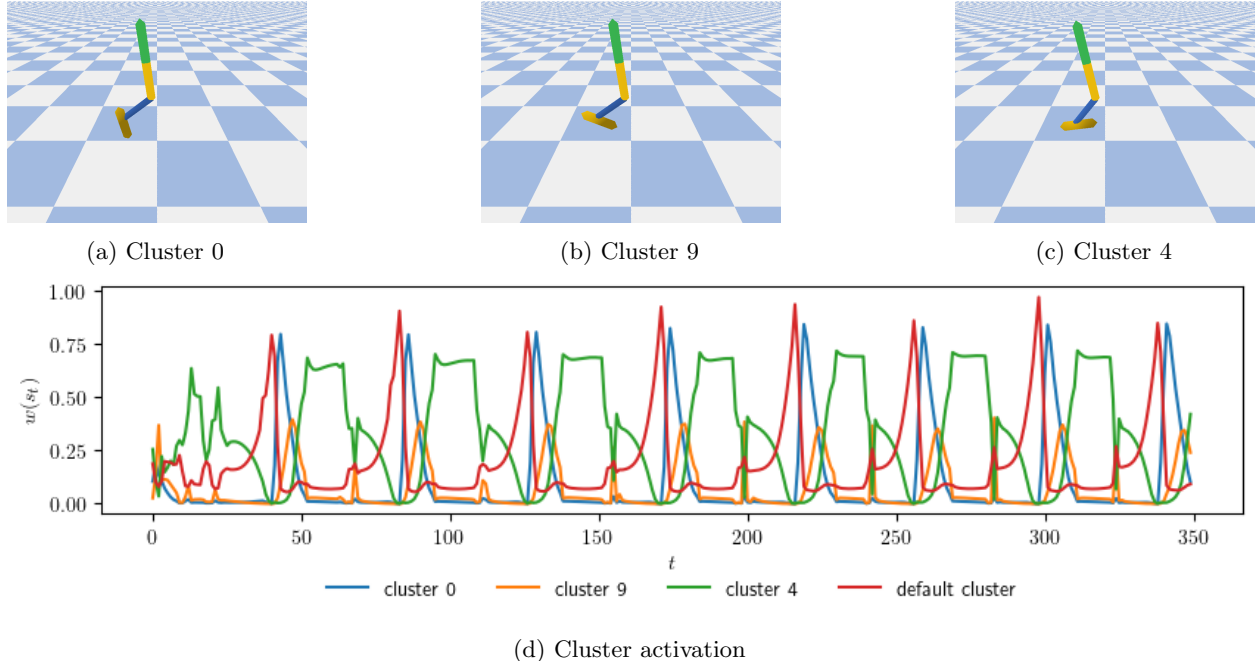


Figure 3: Four cluster out of twenty and their associated activation on the `HopperBulletEnv-v0` environment.

solid line is the mean over the runs and the shaded area is the 95% confidence interval of the mean. The plots displayed were obtained by running 5 evaluation rollouts after each policy update for each algorithm.

Performance. On smaller scale problems shown in Fig. 1 TRPO with a neural network performs best, albeit as the number of clusters increases to 20 we are able to approach the performance of neural network policies. When comparing to a linear policy, our algorithm has significantly higher performance with as little as 5 clusters. On the higher dimensional locomotion tasks, shown in Fig. 2, our algorithm is able to match the performance of TRPO and PPO despite having less parameters, but largely outperforms TRPO with a linear policy. This shows that in the space of interpretable policies, the structure proposed in this paper offers a competitive alternative to linear policies. On a task by task comparison, our algorithm performs especially well on the `AntBulletEnv-v0` environment where it consistently learns walking policies with 10 cluster centers and largely outperforms the baselines with 40 clusters. On this environment our policy only has 1488, 748 and 378 parameters for 40, 20 and 10 clusters respectively whereas the neural network has policy has 6544 and the linear policy 232 parameters. Our algorithm is also able to learn policies competitive with neural network ones on `HopperBulletEnv-v0` with only 20 clusters, while 40 are required to edge out PPO on `HalfCheetahBulletEnv-v0` and come close to TRPO. On `Walker2DBulletEnv-v0`, albeit performance is not too far off of the baselines, it is the only environment where we did not manage to learn a walking gait with up to 40 clusters and the policies only learn to stabilize the agent. We do not believe that this is directly related to the dimensionality of the problem since `AntBulletEnv-v0` is higher dimensional and `HalfCheetahBulletEnv-v0` is only slightly lower dimensional and in both environments, walking gaits can be learned with only 10 clusters.

Interpretability. Fig. 3 and 4 show a subset of the clusters of a policy learned on `HopperBulletEnv-v0` and `HalfCheetahBulletEnv-v0` and their respective activation during a rollout. Clusters are selected if they have high activation and small cross-overlap. Details on the selection methodology of the clusters is detailed in the appendix. In both figures, the cyclical nature of the movement is clearly visible from the activation and the cluster centers show how the movement is decomposed into smaller sub-policies. The best format for understanding the movement decomposition is by inspecting the clusters in animated format, as a static image can represent the cluster center but not its associated action. In Fig. 3 and Fig. 4, we show the cluster centers and provide an animated visualization of the clusters in the supplementary. The animated images are obtained by executing the policy starting from the cluster center for 5 time-steps. By visually inspecting the

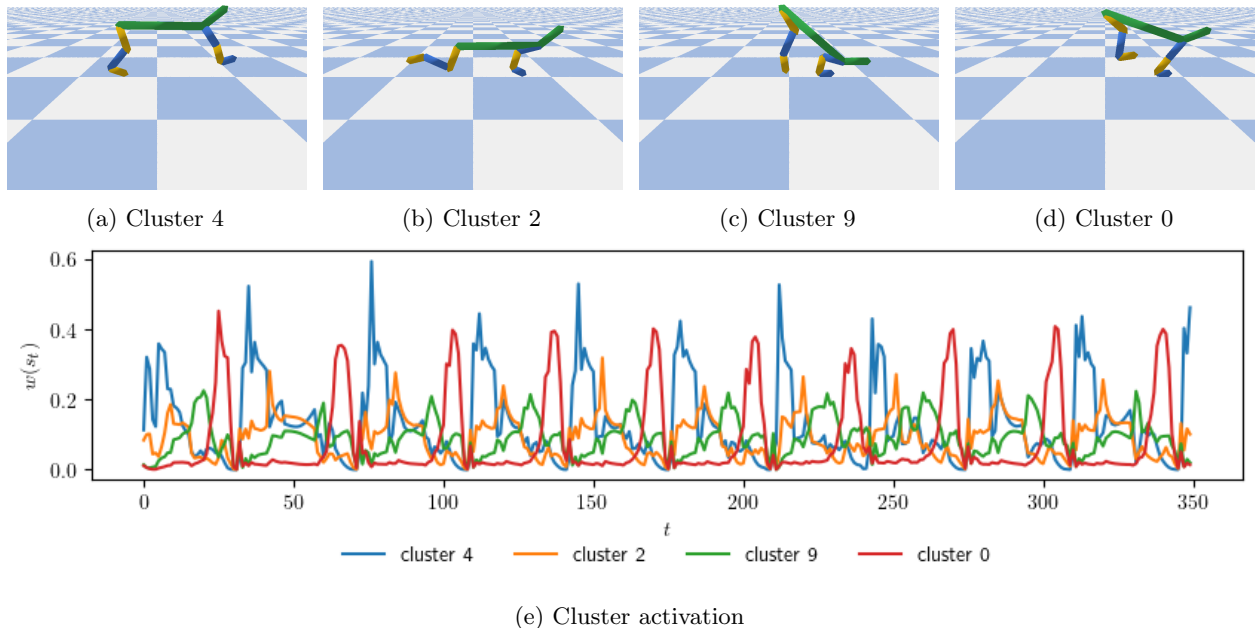


Figure 4: Four cluster out of ten and their associated activation on the `HalfCheetahBulletEnv-v0` environment.

cluster centers it becomes clear that Cluster 4 is responsible for the landing, Cluster 0 the propelling and Cluster 9 rotates the ankle’s joint right after the propelling. Cluster 0 (propelling) is executed in a short burst, and Cluster 4 (landing) is executed the longest as the Hopper spends most of its time in the air. And the motion repeats cyclically, by chaining the propelling, the rotation of the ankle and the landing. The movement of the HalfCheetah is slightly more complex and is decomposed into 4 main parts. The animated visualization of the clusters is provided in the supplementary. In the learned policy shown in Fig. 4, two clusters are responsible for the landing and two clusters for the propelling. The landing operates by extending the rightmost leg (Cluster 4) and slightly thereafter the leftmost leg (Cluster 2), The propelling is done in the opposite order starting with the leftmost leg (Cluster 9) then the right most one (Cluster 0), and the cycle repeats. A similar inspection of the clusters of the higher dimensional Ant problem can give a clear understanding of how the motion can be decomposed. We defer its explanation to the supplementary.

7 Conclusion

We have proposed in this paper a new policy structure based on the proximity to a small set of prototypical states. The policy includes a set of discrete variables which renders its optimization challenging. Yet, our experiments demonstrated that this policy and its associated learning algorithm can be competitive with neural network policies and significantly outperforms linear policies, while being as or even more interpretable than the latter. An important future direction is to tackle the learning of an interpretable distance between states. A possible lead to ensure interpretability is to ensure that the metric respects the underlying dynamics of the MDP, and the intuitive knowledge of which states are likely to come after which other states. While to be able to solve complex tasks such as the Rubik’s cube with a small number of prototypes, the metric needs to learn a more abstract and factored knowledge of the state space.

References

- [1] Richard S. Sutton and Andrew G. Barto. *Reinforcement Learning: An Introduction*. MIT Press, Boston, MA, 1998.
- [2] Csaba Szepesvari. *Algorithms for Reinforcement Learning*. Morgan & Claypool, 2010.
- [3] Volodymyr Mnih, Koray Kavukcuoglu, David Silver, Andrei A. Rusu, Joel Veness, Marc G. Bellemare, Alex Graves, Martin Riedmiller, Andreas K. Fidjeland, Georg Ostrovski, Stig Petersen, Charles Beattie, Amir Sadik, Ioannis Antonoglou, Helen King, Dhharshan Kumaran, Daan Wierstra, Shane Legg, and Demis Hassabis. Human-level control through deep reinforcement learning. *Nature*, 518(7540):529–533, 02 2015.
- [4] David Silver, Aja Huang, Chris J. Maddison, Arthur Guez, Laurent Sifre, George van den Driessche, Julian Schrittwieser, Ioannis Antonoglou, Veda Panneershelvam, Marc Lanctot, Sander Dieleman, Dominik Grewe, John Nham, Nal Kalchbrenner, Ilya Sutskever, Timothy Lillicrap, Madeleine Leach, Koray Kavukcuoglu, Thore Graepel, and Demis Hassabis. Mastering the game of Go with deep neural networks and tree search. *Nature*, 529(7587):484–489, January 2016.
- [5] Timothy P. Lillicrap, Jonathan J. Hunt, Alexander Pritzel, Nicolas Heess, Tom Erez, Yuval Tassa, David Silver, and Daan Wierstra. Continuous control with deep reinforcement learning. *CoRR*, 2015.
- [6] Hado Van Hasselt, Arthur Guez, and David Silver. Deep reinforcement learning with double q-learning. In *Thirtieth AAAI Conference on Artificial Intelligence*, 2016.
- [7] Volodymyr Mnih, Adrià Puigdomènech Badia, Mehdi Mirza, Alex Graves, Timothy P. Lillicrap, Tim Harley, David Silver, and Koray Kavukcuoglu. Asynchronous methods for deep reinforcement learning. In *International Conference on Machine Learning (ICML)*, 2016.
- [8] John Schulman, Sergey Levine, Michael Jordan, and Pieter Abbeel. Trust Region Policy Optimization. *International Conference on Machine Learning (ICML)*, page 16, 2015.
- [9] Ioannis Rexakis and Michail G Lagoudakis. Classifier-based policy representation. In *Seventh International Conference on Machine Learning and Applications*, pages 91–98. IEEE, 2008.
- [10] Charles W Anderson. Approximating a policy can be easier than approximating a value function. *Computer Science Technical Report*, 2000.
- [11] Lihong Li, Thomas J. Walsh, and Michael L. Littman. Towards a unified theory of state abstraction for mdps. In *International Symposium on Artificial Intelligence and Mathematics (ISAIM)*, 2006.
- [12] David Abel, D. Ellis Hershkowitz, and Michael L. Littman. Near optimal behavior via approximate state abstraction. In *International Conference on Machine Learning (ICML)*, pages 2915–2923, 2016.
- [13] Daniel J. Mankowitz, Timothy Arthur Mann, and Shie Mannor. Adaptive skills adaptive partitions (ASAP). In *Advances in Neural Information Processing Systems (NIPS)*, pages 1588–1596, 2016.
- [14] Riad Akrouf, Filipe Veiga, Jan Peters, and Gerhard Neumann. Regularizing reinforcement learning with state abstraction. In *International Conference on Intelligent Robots and Systems (IROS)*, 2018.
- [15] Erik Strumbelj and Igor Kononenko. An efficient explanation of individual classifications using game theory. *Journal of Machine Learning Resource (JMLR)*, 2010.
- [16] Marco Tulio Ribeiro, Sameer Singh, and Carlos Guestrin. ”why should i trust you?”: Explaining the predictions of any classifier. In *Knowledge Discovery and Data Mining (KDD)*, 2016.
- [17] Mark Craven and Jude W. Shavlik. Extracting tree-structured representations of trained networks. In *Advances in Neural Information Processing Systems (NIPS)*, 1996.
- [18] Berk Ustun and Cynthia Rudin. Supersparse linear integer models for optimized medical scoring systems. *Machine Learning*, 2015.

- [19] Benjamin Letham, Cynthia Rudin, Tyler H. McCormick, and David Madigan. Interpretable classifiers using rules and bayesian analysis: Building a better stroke prediction model. *The Annals of Applied Statistics*, 2015.
- [20] Ashish Vaswani, Noam Shazeer, Niki Parmar, Jakob Uszkoreit, Llion Jones, Aidan N Gomez, Łukasz Kaiser, and Illia Polosukhin. Attention is all you need. In *Advances in Neural Information Processing Systems (NIPS)*, 2017.
- [21] Prashan Madumal, Tim Miller, Liz Sonenberg, and Frank Vetere. Explainable reinforcement learning through a causal lens. In *Conference on Artificial Intelligence (AAAI)*, 2019.
- [22] Bradley Hayes and Julie A. Shah. Improving robot controller transparency through autonomous policy explanation. In *International Conference on Human-Robot Interaction (HRI)*, 2017.
- [23] Abhinav Verma, Vijayaraghavan Murali, Rishabh Singh, Pushmeet Kohli, and Swarat Chaudhuri. Programmatically interpretable reinforcement learning. In *International Conference on Machine Learning (ICML)*, 2018.
- [24] Osbert Bastani, Yewen Pu, and Armando Solar-Lezama. Verifiable reinforcement learning via policy extraction. In *Advances in Neural Information Processing Systems (NeurIPS)*, 2018.
- [25] Xinkun Nie, Emma Brunskill, and Stefan Wager. Learning When-to-Treat Policies. *arXiv e-prints*, 2019.
- [26] Stéphane Ross and Drew Bagnell. Efficient reductions for imitation learning. In *AISTATS*, pages 661–668, 2010.
- [27] Damien Ernst, Pierre Geurts, and Louis Wehenkel. Tree-based batch mode reinforcement learning. *Journal of Machine Learning Research*, 2005.
- [28] Youri Coppens, Kyriakos Efthymiadis, Tom Lenaerts, and Ann Nowe. Distilling deep reinforcement learning policies in soft decision trees. In *IJCAI Workshop on Explainable Artificial Intelligence*, 2019.
- [29] Aravind Rajeswaran, Kendall Lowrey, Emanuel Todorov, and Sham M. Kakade. Towards generalization and simplicity in continuous control. In *Conference on Neural Information Processing Systems (NIPS)*, 2017.
- [30] X. Xu, D. Hu, and X. Lu. Kernel-based least squares policy iteration for reinforcement learning. *IEEE Transactions on Neural Networks*, 2007.
- [31] Michail Lagoudakis and Ronald Parr. Least-squares policy iteration. *Journal of Machine Learning Research (JMLR)*, 4:1107–1149, 2003.
- [32] Dimitri P. Bertsekas. Approximate policy iteration: a survey and some new methods. *Journal of Control Theory and Applications*, 9(3):310–335, Aug 2011.
- [33] Bruno Scherrer. Approximate policy iteration schemes: A comparison. In *Proceedings of the 31th International Conference on Machine Learning, ICML 2014, Beijing, China, 21-26 June 2014*, pages 1314–1322, 2014.
- [34] John Schulman, Philipp Moritz, Sergey Levine, Michael I. Jordan, and Pieter Abbeel. High-dimensional continuous control using generalized advantage estimation. In *4th International Conference on Learning Representations, ICLR 2016*, 2016.
- [35] Lotfi A Zadeh. Fuzzy sets. *Information and control*, 8(3):338–353, 1965.
- [36] Saeed Masoudnia and Reza Ebrahimpour. Mixture of experts: A literature survey. *Artif. Intell. Rev.*, 2014.
- [37] John Schulman, Filip Wolski, Prafulla Dhariwal, Alec Radford, and Oleg Klimov. Proximal policy optimization algorithms. *CoRR*, abs/1707.06347, 2017.

- [38] John L Bresina. Heuristic-biased stochastic sampling. In *AAAI/IAAI, Vol. 1*, pages 271–278, 1996.
- [39] Riad Akrou, Joni Pajarinen, Jan Peters, and Gerhard Neumann. Projections for approximate policy iteration algorithms. In *International Conference on Machine Learning (ICML)*, 2019.
- [40] Erwin Coumans and Yunfei Bai. Pybullet, a python module for physics simulation for games, robotics and machine learning. <http://pybullet.org>, 2016–2019.
- [41] Emanuel Todorov, Tom Erez, and Yuval Tassa. Mujoco: A physics engine for model-based control. In *International Conference on Intelligent Robots and Systems (IROS)*, pages 5026–5033. IEEE, 2012.
- [42] Sham M Kakade. A natural policy gradient. In *Advances in neural information processing systems (NIPS)*, pages 1531–1538, 2002.
- [43] J. Peters and S. Schaal. Natural Actor-Critic. *Neurocomputation*, 71(7-9):1180–1190, 2008. ISSN 0925-2312.
- [44] Prafulla Dhariwal, Christopher Hesse, Oleg Klimov, Alex Nichol, Matthias Plappert, Alec Radford, John Schulman, Szymon Sidor, and Yuhuai Wu. Openai baselines. <https://github.com/openai/baselines>, 2017.

A Policy interpretation from cluster center visualization

We show in this section how learned gaits can be interpreted as the repeated application of simpler movements. We show that this process is made much easier thanks to the visualization of the cluster centers and their associated action, learned with our algorithm. A simple experiment to reinforce this claim is to first look at rollouts of the gait, provided in the supplementary material, without visualizing the clusters, attempting a first interpretation of the gait and then formulating a second interpretation after visualizing the cluster centers. The benefits of our interpretable policy is especially evident as the complexity of the task increases, such as with the Ant, where the movement requires the synchronized actuation of several joints of the agent.

As discussed in the paper, the policy is better understood when visualizing the cluster centers and their associated action in animated format. We showed in the paper a selection of cluster centers that give an idea of the ‘pose’—i.e. joint configuration—of the agent. However, in the animated `gifs` in the supplementary, a much clearer understanding of the learned policy can be gained; as the animated nature allows to additionally see joint velocities and most importantly the associated action to each cluster center.

We provide in this appendix a walk-through of the protocol we have followed to understand the gaits of the interpretable policies learned on both the `AntBulletEnv-v0` and the `HalfCheetahBulletEnv-v0` environments. Starting with the Ant, we first pick the best policy out of the 25 runs of our algorithm with 10 clusters. Next, we perform a rollout with the deterministic policy—i.e. with no exploration noise—and collect the cluster activations w along time. All cluster activations can be seen in Fig. 5. Clearly from Fig. 5, the clusters with clear high peaks are 4 and 6. Having identified two main clusters, we look for clusters that activate when 4 and 6 do not, and select 5 and 2 accordingly. Note that there are clusters that do not activate evenly and in a cyclic manner during the rollout. For instance, Cluster 9 is only active in the first few time steps. As the Ant starts the episode falling from a distance, it is natural that a different set of clusters are responsible for the landing, and their inspection could be of interest if one desires to understand this phase. However, we are interested here in the cyclic gait movement that starts around time-step 70 and for which Clusters 5, 4, 6 and 2 activate with the highest intensity and regularity.

Having identified the main clusters, we now proceed to their visualization in animated format. We do so by setting the environment to each of the selected clusters and repeatedly executing their associated action for 5 time-steps, and recording an animated gif for each cluster that can be found in the supplementary material. The clusters are saved following the order with which they are executed in the policy, as can be seen in Fig. 5. Visualizing the clusters shows that the Ant walks by moving two opposed legs at a time, which is the responsibility of Cluster 5 and 6. While the Ant executes Cluster 5 (rotation of the first pair of legs) it initiates Cluster 4 which is responsible for rotating the Ant counter-clockwise. Similarly, while the Ant executes Cluster 6 (rotation of the other pair of legs) it executes Cluster 2 which pulls a previously extended leg back. When watching a rollout of the learned policy, that can also be found in the supplementary material, the clusters and their execution sequence as described here can clearly be identified when the Ant is past the ‘transient’ phase of the rollout after the first circa 70 time-steps.

We repeat the same protocol for understanding the gait in the `HalfCheetahBulletEnv-v0` environment. Fig. 6 shows the cluster activations and the selected clusters. After visualization of the selected cluster centers, we conjecture that the learned gait of the `HalfCheetah` proceeds with the following structure. There are two clusters responsible for the landing and two clusters for the propelling. The landing operates by extending the rightmost leg (Cluster 4) and slightly thereafter the leftmost leg (Cluster 2). The propelling is done in the opposite order starting with the leftmost left (Cluster 9) then the right most one (Cluster 0), and the cycle repeats.

B Derivation of KL bounds for cluster weights projections

We present the derivations for the KL bounds for our interpretable policies. We use the following projections:

$$\begin{aligned}c_\eta &= \eta c + (1 - \eta)c_q \\M_\nu &= \nu M + (1 - \nu)M_q \\ \Sigma_\kappa &= \kappa \Sigma + (1 - \kappa)\Sigma_q\end{aligned}\tag{9}$$

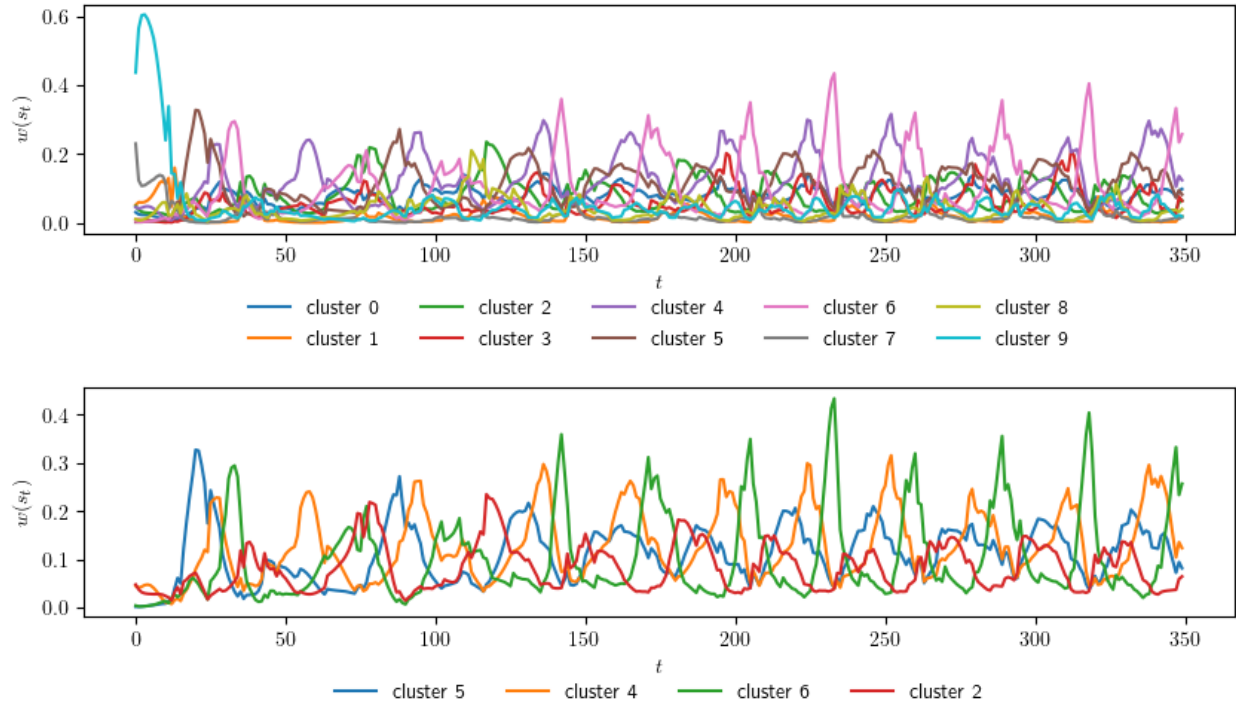


Figure 5: Top: all cluster activations for a rollout on the `AntBulletEnv-v0` environment with a 10 cluster center interpretable policy. Bottom: selected subset of 4 clusters that have largest spikes and least overlap.

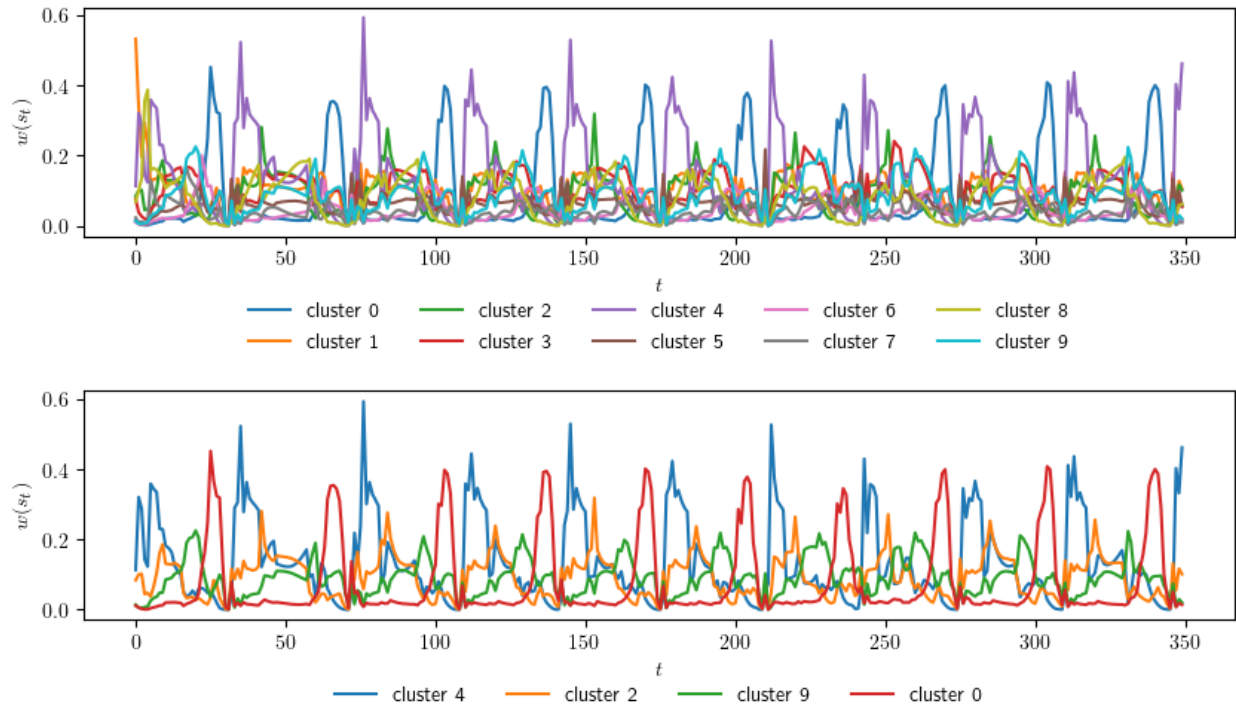


Figure 6: Top: all cluster activations for a rollout on the `HalfCheetahBulletEnv-v0` environment with a 10 cluster center interpretable policy. Bottom: selected subset of 4 clusters that have largest spikes and least overlap.

As discussed in the paper, the cluster actions and cluster weights only affect the mean component of the KL divergence, while Σ only affects the entropy and rotation component. The cluster weights projection can be seen equivalently in the unnormalized cluster membership space:

$$w_\eta = \eta w + (1 - \eta)w_q \quad (10)$$

Keeping the same notation as the paper, we bound the mean component of the KL divergence, which can be written in the following way in terms of change in cluster action and cluster weights

$$m(\nu, \eta) = \left\| M_\nu \frac{w_\eta}{\|w_\eta\|_1} - M_q \frac{w_q}{\|w_q\|_1} \right\|_{\Sigma_q^{-1}}^2, \quad (11)$$

$$= \left\| (\nu M + (1 - \nu)M_q) \frac{w_\eta}{\|w_\eta\|_1} - M_q \frac{w_q}{\|w_q\|_1} \right\|_{\Sigma_q^{-1}}^2, \quad (12)$$

$$= \left\| \nu (M - M_q) \frac{w_\eta}{\|w_\eta\|_1} + M_q \left(\frac{w_\eta}{\|w_\eta\|_1} - \frac{w_q}{\|w_q\|_1} \right) \right\|_{\Sigma_q^{-1}}^2, \quad (13)$$

$$= \nu^2 \left\| (M - M_q) \frac{w_\eta}{\|w_\eta\|_1} \right\|_{\Sigma_q^{-1}}^2 + 2\nu \left((M - M_q) \frac{w_\eta}{\|w_\eta\|_1} \right)^T \Sigma_q^{-1} \left(M_q \left(\frac{w_\eta}{\|w_\eta\|_1} - \frac{w_q}{\|w_q\|_1} \right) \right) + \left\| M_q \left(\frac{w_\eta}{\|w_\eta\|_1} - \frac{w_q}{\|w_q\|_1} \right) \right\|_{\Sigma_q^{-1}}^2. \quad (14)$$

In order to compute the projection we start by setting $\nu = 0$. Thus we obtain:

$$m(\eta, 0) = \left\| M_q \left(\frac{w_\eta}{\|w_\eta\|_1} - \frac{w_q}{\|w_q\|_1} \right) \right\|_{\Sigma_q^{-1}}^2. \quad (15)$$

We can rewrite this term as follows:

$$\begin{aligned} m(\eta, 0) &= \left(M_q \frac{\eta w + (1 - \eta)w_q}{\|\eta w + (1 - \eta)w_q\|_1} - M_q \frac{w_q}{\|w_q\|_1} \right)^T \Sigma_q^{-1} \left(M_q \frac{\eta w + (1 - \eta)w_q}{\|\eta w + (1 - \eta)w_q\|_1} - M_q \frac{w_q}{\|w_q\|_1} \right) \\ &= \left(\frac{\eta w + (1 - \eta)w_q}{\|\eta w + (1 - \eta)w_q\|_1} - \frac{w_q}{\|w_q\|_1} \right)^T M_q^T \Sigma_q^{-1} M_q \left(\frac{\eta w + (1 - \eta)w_q}{\|\eta w + (1 - \eta)w_q\|_1} - \frac{w_q}{\|w_q\|_1} \right) \\ &= \left\| \frac{\eta w + (1 - \eta)w_q}{\|\eta w + (1 - \eta)w_q\|_1} - \frac{w_q}{\|w_q\|_1} \right\|_{M_q^T \Sigma_q^{-1} M_q}^2 \\ &= \left\| \frac{\eta w \|w_q\|_1 + (1 - \eta)w_q \|w_q\|_1 - w_q \|\eta w + (1 - \eta)w_q\|_1}{\|\eta w + (1 - \eta)w_q\|_1 \|w_q\|_1} \right\|_{M_q^T \Sigma_q^{-1} M_q}^2 \\ &= \left\| \frac{\eta w \|w_q\|_1 + (1 - \eta)w_q \|w_q\|_1 - \eta w_q \|w\|_1 - (1 - \eta)w_q \|w_q\|_1}{\|\eta w + (1 - \eta)w_q\|_1 \|w_q\|_1} \right\|_{M_q^T \Sigma_q^{-1} M_q}^2 \\ &= \left\| \frac{\eta w \|w_q\|_1 - \eta w_q \|w\|_1}{\|\eta w + (1 - \eta)w_q\|_1 \|w_q\|_1} \right\|_{M_q^T \Sigma_q^{-1} M_q}^2 \\ &= \frac{\eta^2}{\|\eta w + (1 - \eta)w_q\|_1^2} \left\| \frac{w \|w_q\|_1 - w_q \|w\|_1}{\|w_q\|_1} \right\|_{M_q^T \Sigma_q^{-1} M_q}^2 \\ &= \frac{\eta^2 \|w\|_1^2}{\|\eta w + (1 - \eta)w_q\|_1^2} \left\| \frac{w}{\|w\|_1} - \frac{w_q}{\|w_q\|_1} \right\|_{M_q^T \Sigma_q^{-1} M_q}^2 \\ &= \frac{\eta^2 \|w\|_1^2}{\|\eta w + (1 - \eta)w_q\|_1^2} m(1, 0). \end{aligned} \quad (16)$$

We bound Eq. (16) with:

$$m(\eta, 0) \leq \begin{cases} \eta^2 \frac{\|w\|_1^2}{\|w_q\|_1^2} m(w) & \|w\|_1 \geq \|w_q\|_1 \\ \eta^2 m(w) & \text{otherwise} \end{cases} \quad (17)$$

We can write the bound compactly as:

$$m(\eta, 0) \leq \eta^2 \max\left(\frac{\|w\|_1^2}{\|w_q\|_1^2}, 1\right) m(w) \quad (18)$$

We can derive a second bound using convexity of $\|w_\eta\|_1^2$ in η . Let $f(\eta) = \|w_\eta\|_1^2$, then

$$\begin{aligned} f(\eta) &\geq f(0) + f'(0)\eta \\ &= \|w_q\|_1^2 + 2\|w_q\|_1(\|w\|_1 - \|w_q\|_1)\eta \\ &\geq \eta(\|w_q\|_1^2 + 2\|w_q\|_1(\|w\|_1 - \|w_q\|_1)) \\ &= \eta(2\|w_q\|_1\|w\|_1 - \|w_q\|_1^2) \end{aligned}$$

If the r.h.s. of the inequality is positive, this gives rise to this alternative upper bound

$$m(\eta) \leq \eta \frac{\|w\|_1^2}{2\|w_q\|_1\|w\|_1 - \|w_q\|_1^2} m(1)$$

If $\|w\| \approx \|w_q\|$ the previous bound is tighter. If $\|w\| \gg \|w_q\|$ the second bound is preferable.

As both these inequalities are simple in η , they can be used to solve for η in order to make sure $m(\eta, 0) \leq \epsilon$, as required by the KL-divergence constraint. After a good value for η has been found, we can easily find a value for ν by solving the quadratic inequality in ν after fixing η .

C Pseudocode of auxiliary procedures

We present the pseudocode for the auxiliary routines presented in the paper.

The `polynomialSample` procedure performs the randomization scheme described in [38]. Let $r(c)$ be the ranking function that, for every candidate, returns the position in the vector ordered by descending order w.r.t. a given heuristic h . The probability of sampling a given candidate, up to a normalizing factor, is:

$$p(c) \propto \frac{1}{r(c)^\delta}.$$

The parameter δ can be used to tune the probability distribution: higher values of δ correspond to a shift of the probability distribution towards the most promising samples. In our experiments, we set always δ to 1.

The `createNewPolicy` function takes as input a starting policy, a set of cluster centers and a set of indexes, and creates a new policy where the cluster centers at the given indices are exchanged with the provided ones. If also actions are provided, the function will update the action correlated with the cluster.

The cluster optimization routine is presented in Alg. 3. At each iteration, the value of the maximum number of swaps $n_{\text{swaps max}}$ is set to the one used in the previous call of the routine. If the last swap attempt has been successful, we multiply $n_{\text{swaps max}}$ by 1.8. If $n_{\text{swaps max}} < 1$, then we set it to 1 for the next iteration. The first call of the `swapCluster` routine uses $n_{\text{swaps max}} = K$.

Algorithm 2 addClusters Routine

- 1: **Input:** policy q , trajectories \mathcal{T} , advantage function A
 - 2: clusters, actions \leftarrow `getHighAdvantageClusters`(\mathcal{T}, A)
 - 3: $\pi \leftarrow$ `createNewPolicy`(π , indexes, clusters, action)
 - 4: **return** π
-

Algorithm 3 swapCluster Routine

- 1: **Input:** policy q , trajectories \mathcal{T}
 - 2: $h_1, h_2 =$ `computeHeuristics`(q, \mathcal{T})
 - 3: $\pi_{\text{max}} \leftarrow q$
 - 4: $\mathcal{J}_{c \text{ max}} \leftarrow$ `computeObjective`(q, \mathcal{T})
 - 5: $n_{\text{swaps}} \leftarrow n_{\text{swaps max}}$
 - 6: **while** $n_{\text{swaps}} \geq 1$ **and** $\pi_{\text{max}} = q$ **do**
 - 7: **for** $i = 0$ **to** n **do**
 - 8: indexes \leftarrow `polynomialSample`($h_1, \lceil n_{\text{swaps}} \rceil$)
 - 9: candidates \leftarrow `polynomialSample`($h_1, \lceil n_{\text{swaps}} \rceil$)
 - 10: $\pi \leftarrow$ `createNewPolicy`(q , indexes, candidates)
 - 11: **if** $\text{KL}(\pi(\cdot|s) \parallel q(\cdot|s)) \leq \epsilon$ **then**
 - 12: $\mathcal{J}_c \leftarrow$ `computeObjective`(π, \mathcal{T})
 - 13: **if** $\mathcal{J}_c \geq \mathcal{J}_{c \text{ max}}$ **then**
 - 14: $\pi_{\text{max}} \leftarrow \pi$
 - 15: $\mathcal{J}_{c \text{ max}} \leftarrow \mathcal{J}_c$
 - 16: **end if**
 - 17: **end if**
 - 18: **end for**
 - 19: $n_{\text{swaps}} \leftarrow n_{\text{swaps}}/2$
 - 20: **end while**
 - 21: **return** π_{max}
-

The compression routine is presented in Alg. 4. The `sortClusterCenters` returns the cluster centers of the policy, sorted by ascending magnitude of cluster weight, and the corresponding indexes. The rationale behind this choice is that a higher cluster weight corresponds to a cluster that is more important for the policy, and thus is less likely to be a redundant cluster. The compression consists of setting to zero the irrelevant cluster weights and substitute them with clusters with high advantage. Note that, since the KL bound is respected when setting the cluster weight to zero, it is also possible to exchange the deactivated cluster with any other cluster center and action, as this change has no effect on the policy distribution.

D Experimental settings

We present the set of hyperparameters used in our experiments. Every run is composed by a fixed number of epochs: 1000 epochs for the Bullet walking environments (HopperBulletEnv-v0, Walker2DBulletEnv-v0, HalfCheetahBulletEnv-v0, and AntBulletEnv-v0) and 500 for the remaining environments (BipedalWalker-v2, Pendulum-v0, and InvertedPendulumBulletEnv-v0). Every epoch consist of collecting 3008 steps in the environment and a policy update. After the policy update we perform 5 episodes of evaluation (the trajectories extracted are not used for learning). For every environment, gamma is set to 0.99.

All deep learning comparison experiments has been performed using OpenAI baselines implementation. We added the evaluation of the policy after each policy update to the original codebase.

The algorithms used in the experimental section of this work use the following parameters:

TRPO

- Network:
 - TRPO (MLP): Feed Forward Neural network with 2 hidden layers of 64 neurons.
 - TRPO (Linear): Linear in the state policy with bias parameters.
- maximum KL during policy updates: 0.01 (effective maximum KL of 0.015 as the maximum KL hyper-parameter is multiplied by 1.5 during the linesearch in the default OpenAI implementation.)
- Conjugate gradient parameters:
 - number of iterations: 10
 - damping: 0.1
- Value function parameters:
 - number of updates iterations: 5
 - optimizer stepsize: 1e-3
 - GAE lambda coefficient: 0.95

PPO

- Network: Feed Forward Neural network with 2 hidden layers of 64 neurons.
- number of minibatches: 64
- number of training epochs per update: 10
- number of optimizations per epoch: 10
- clipping range parameter: 0.2
- entropy coefficient: 0.0
- GAE lambda coefficient: 0.95
- learning rate: linearly decreasing learning rate with slope constant 3e-4

Algorithm 4 compressPolicy Routine

```
1: Input: policy  $q$ , trajectories  $\mathcal{T}$ , advantage function  $A$ 
2:  $\pi \leftarrow q$ 
3:  $i \leftarrow 0$ 
4:  $\pi_i \leftarrow q$ 
5:  $c_{\text{sorted}}, \text{indexes} \leftarrow \text{sortClusterCenters}(q)$ 
6: while  $\text{KL}(\pi(\cdot|s) \parallel q(\cdot|s)) \leq \epsilon$  do
7:    $\pi \leftarrow \pi_i$ 
8:    $c_{\text{sorted}}[i] \leftarrow 0$ 
9:    $\pi_i \leftarrow \text{createNewPolicy}(q, \text{indexes}_{c_{\text{sorted}}})$ 
10:   $i \leftarrow i + 1$ 
11: end while
12: if  $\pi \neq q$  then
13:    $\text{indexes}, \text{clusters}, \text{actions} \leftarrow \text{getHighAdvantageClusters}(\mathcal{T}, A)$ 
14:    $\pi \leftarrow \text{createNewPolicy}(\pi, \text{indexes}, \text{clusters}, \text{action})$ 
15: end if
16: return  $\pi$ 
```

Metric RL

- Policy:
 - Initial standard deviation: 1.0
 - Cluster temperature: 0.33 for HalfCheetahBulletEnv-v0 and AntBulletEnv-v0, 1.0 for the others tasks.
- Actor optimizer:
 - Optimizer: Adam
 - cluster learning rate: 0.01
 - mean learning rate: 0.01
 - variance learning rate: .001
 - entropy profile: Two phases entropy profile, unconstrained until the entropy has reached 50% of initial policy entropy; after the threshold is reached the entropy bound decreases linearly with constant 0.0075.
 - Update epochs per fit: 20,
 - Batch size: 64.
 - maximum KL during policy updates: .015.
- Critic Params
 - Network: Feed Forward Neural network with 2 hidden layers of 64 neurons.
 - Optimizer: Adam, with learning rate 3e-4.
 - batch size for update: 64
 - GAE lambda coefficient: 0.95
 - 2 models for the critic update, using min operator to compute the target.
 - Update epochs per fit: 10.